# Lipid Hydrolysis in Lung Cancer Metabolism

Scientific Research Paper

On behalf of the Austrian Marshall Plan Foundation Scholarship Program

By Sophie Elisabeth Honeder, MSc.

April 4th, 2022 – March 3rd, 2023

**SUPERVISORS**

**Host Institution: Prof. Matthew Vander Heiden, MD, PhD**

Department of Biology

Koch Institute of Integrative Cancer Research

Massachusetts Institute of Technology

**Home Institution: Prof. Ruth Birner-Grünberger, PhD**

Institute of Pathology

Medical University of Graz

and

Institute of Chemical Technologies and Analytics,

TU Wien

# Table of Contents

# Abstract

Cancer cells frequently undergo sophisticated metabolic changes in order to maintain a proliferative phenotype in challenging environments. Already in the 1920s, Otto Warburg reported of alterations of glucose usage in cancer cells, and thus paved the way for a new research field: cancer metabolism. Most cancer (and highly proliferative) cells preferably ferment pyruvate into lactate despite oxygen availability (aerobic glycolysis), and glucose metabolism has been in the center of cancer metabolism research for decades. More recently, lipid metabolism in cancer has gained interest, and fatty acid metabolism has been described as a key player in progression of cancer. Cancer cells often display increased de-novo fatty acid synthesis and fatty acid uptake. Lipid catabolism on the other hand is a less well-studied process in the context of cancer but has recently been brought into the picture of cancer formation and progression. However, its role in cancer metabolism is not yet fully understood. A major enzyme of triglyceride catabolism in the cell is adipose triglyceride lipase (ATGL), which catalyzes the first and rate-limiting step of the breakdown of triglycerides that are stored in lipid droplets within the cells. ATGL has recently been proposed to play a role in lung cancer. Another lipase involved in intracellular lipid degradation – monoglyceride lipase (MGL) – plays a role in signaling and has been shown to influence cancer pathogenesis.

Therefore, the aim of this study is to investigate enzymes involved in intracellular lipid catabolism, such as ATGL and MGL, and their influence on cancer progression and metabolism.

We previously reported that knocking out ATGL in a non-small cell lung cancer cell line – A549 – led to increased proliferation and migration in 2D cell culture. Strikingly, in 3D

cell culture, an even more significant growth and morphology difference was observed between A549 ATGL-KO multicellular tumor spheroids and the corresponding control spheroids. Proteomic analysis of the A549 ATGL-KO spheroids and A549 control spheroids revealed changes in glucose and fatty acid metabolism. These findings were corroborated by increased expression of glucose transporters as well as higher lactate and lower glucose levels in the medium of lipolysis-deficient cell lines and higher levels of monounsaturated fatty acids.

The aim of this research stay is to generate a panel of lung cancer cell lines with different genetic backgrounds and deletion of ATGL or MGL. Furthermore, the aim is to test the phenotype of these cell lines and the influence of lipolysis deficiency in the different cell lines on proliferation. Furthermore, metabolic tracing by employing stable-isotope labeled metabolites should be applied to gain more insight into how lipolysis deficiency influences metabolism in the generated cell lines.

# 1. Introduction

## 1.1. Lung cancer

Cancer is among the leading causes of death worldwide and remains to be one of the greatest barriers to increased life expectancy. Due to inadequate early diagnosis, lung cancer tops the list of cancers that cause the most deaths, annually accounting for nearly 1.8 million fatalities worldwide [1].

Taking into account data from both females and males worldwide, lung cancer is responsible for the highest number of new cancer cases (11.6%) among all types of cancer. In 2018, approximately 2.1 million individuals received a diagnosis of lung cancer [1]. Breast cancer, on the other hand, is the most common cancer among women, accounting for almost a quarter of all newly diagnosed cancers in women. Unfortunately, the prognosis for lung cancer is poor, with a lower chance of survival, and it thus caused 1.8 million deaths in 2018, comprising 18.4% of all cancer-related fatalities [1].

One of the main challenges associated with lung cancer is its complexity and heterogeneity, even within similar subtypes [2]. Another significant issue is the difficulty in early detection, which contributes to its high mortality rate worldwide. Lung cancer often goes unnoticed in its early stages, emphasizing the urgent need for new diagnostic tools that can identify it earlier. Tumor markers, substances typically measured in body fluids like urine or blood, offer a promising approach for diagnosing or predicting the prognosis of certain cancers. However, the availability of cancer-specific tumor markers is crucial for their effective use. Nowadays, the expression patterns of tumor suppressor genes or proto-oncogenes are frequently utilized to test for the presence of cancer [3].

Lung cancer can be classified histologically into two main groups: small cell lung carcinoma (SCLC) and non-small cell lung carcinoma (NSCLC). Among these, NSCLC accounts for approximately 85% of all lung cancer cases [4]. NSCLC can be further divided into three subgroups: large cell carcinoma (LCC), squamous cell carcinoma (SqCC), and adenocarcinoma (AdC).

## 1.2. Cancer hallmarks and altered metabolism

Cancer cells arise from normal cells through genetic alterations that provide them with a growth advantage [5]. These alterations involve mutations in cancer genes, which can be categorized into tumor suppressor genes and oncogenes [5]. Tumor suppressor genes regulate the cell cycle and DNA repair processes [6], while oncogenes promote growth and differentiation [7]. Mutations in these genes contribute to cancer cell advantages. Common characteristics of cancer, known as hallmarks of cancer, include alterations in growth and proliferation signaling, deregulation of the cell cycle, evading apoptotic cell death, maintaining replicative potential, genomic instability, immune modulation, tumor-promoting inflammation, invasion and metastasis, increased vascularization through angiogenesis, and altered energy metabolism. These characteristics support cancer cell survival, growth, and spread [5,8].

A core characteristic of cancer is altered metabolism, through which cancer cells support increased bioenergetic and biosynthetic demands [9]. Changes in metabolism between cancer and normal cells have already been described in the 1920s by Otto Warburg, who discovered that cancer cells preferably ferment glucose into lactate, while normal cells oxidize glucose to CO2 through mitochondrial oxidative phosphorylation [10].

Although this phenomenon was long thought to be due to dysfunctional mitochondria, it is now widely accepted that cancer cells (and other proliferating cells) benefit from altered metabolism, and metabolic switch is now regarded as a separate cancer hallmark [8]. However, metabolism involves not only conversion of glucose, but also the conversion of other nutrients like lipids and proteins. Lipid metabolism in cancer has gained interest in recent years, and fatty acid metabolism has been recognized as a key process in cancer cell proliferation [11].

## 1.3. Lipid metabolism in cancer

Cancer cells rely on fatty acids (FAs) to maintain bioenergetic and biosynthetic needs [12]. Exogenous FAs can be taken up by cancer cells from the tumor microenvironment, while endogenous FAs are generated through de novo synthesis or degradation of triacylglycerol (TAG). TAGs, along with other neutral lipids, are stored in lipid droplets (LDs), which are dynamic organelles composed of a hydrophobic core surrounded by a lipid monolayer [13]. LDs have been observed to accumulate in various types of cancer cells [13]. LDs are associated with lipid-droplet-associated proteins, such as perilipins, which regulate lipid metabolism [14]. LDs are formed through TAG synthesis in the endoplasmic reticulum and are degraded through a process called lipolysis. Lipid hydrolysis enzymes, i.e., lipid hydrolases, play an important role in energy generation by providing fatty acids for mitochondrial beta-oxidation [15]. They also play an important role for protein acylation and they are required for membrane biosynthesis and for the generation of signaling molecules, thereby contributing to cancer cell proliferation [12].

Several enzymes of the intracellular lipid hydrolysis cascade as well as some of their coregulators have been associated with cancer formation and/or progression [16].

Intracellular lipolysis involves the enzymatic activity of adipose triglyceride lipase (ATGL) to produce non-esterified fatty acids (NEFAs) and glycerol [15]. ATGL activity is regulated by CGI-58 and G0S2. The activation of ATGL occurs through the interaction with CGI-58, while G0S2 inhibits ATGL by binding to its N-terminal patatin-domain [15]. Furthermore, ATGL is inhibited by hypoxia-inducible lipid droplet associated protein (HILPDA) in response to hypoxia, causing lipid droplet accumulation, which is often observed in hypoxic tumors and also points towards a tumor suppressor role for ATGL [13,17,18]. Previously it has been shown that loss of ATGL in mice causes spontaneous formation of neoplasia in the lung which often results in lung carcinoma. It has also been shown that ATGL expression is lower in lung cancer tissue compared to healthy lung tissue [19]. However, the role of intracellular lipolysis through ATGL in cancer development and progression is still under debate and the involvement of ATGL cofactors, including HILPDA and CGI-58, further adds complexity to the understanding of ATGL's role in cancer.

The last step of intracellular lipolysis is catalyzed by monoacylglycerol lipase (MGL), which catalyzes the conversion of monoacylglycerols (MGs) to glycerol and fatty acids (FAs). Since both FAs (e.g., arachidonic acid) and MGs (e.g., 2-arachidonoyl-glycerol (2-AG) can act as signaling molecules, MGL is an important enzyme involved in cell signaling [20]. Increased activity of MGL was previously associated with aggressive cancer types, promoting migratory potential, growth, and survival through the generation of pro-tumorigenic signaling molecules [21], while decreased MGL expression in the tumor

microenvironment of NSCLC was reported to slow tumor growth [22]. Another group, however, reported that loss of MGL caused increased incidence of lung cancer in a mouse model [23].

## 1.4. Previous work

We previously tested the effect of aberrant lipolysis through ATGL-KO in a non-small cell lung cancer cell line – A549. Previous experiments of A549 ATGL-KO clones by our lab showed that knockout of ATGL results in accumulation of lipid droplets and changes in the lipidome, as well as increased migration in dependence of SRC activation, which is a known proto-oncogene tyrosine-kinase [16]. These data suggest a tumor suppressor function of ATGL and corroborate that lipid hydrolysis play a role in lung cancer progression. We next investigated metabolic and phenotypic changes in A549 cells upon ATGL-KO in a more in-vivo-like setup by employing 3D cell culture techniques and found a significant proliferation difference between spheroids derived from cells lacking ATGL or derived from control cells [24]. The increase in proliferation dependent on ATGL-KO was more profound in 3D cell culture than in the same cells cultured in 2D cell culture [24]. Glucose and glutamine consumption as well as lactate production was measured and ATGL-KO clones grown in 3D but not in 2D cell culture show significantly more glucose consumption and lactate production than corresponding control clones. LC-MS/MS-based proteomics analysis corroborate the data on glucose uptake and lactate production and reveal higher levels of a glucose transporter as well as glycolytic enzymes in the ATGL-KO cell-derived spheroids. Moreover, proteins involved in lipid metabolism were identified that are changed in ATGL-KO cells, pointing towards lower fatty-acid beta-oxidation and increased production of mono-unsaturated fatty acids [24].

We confirmed changes in the ratio of monounsaturated to saturated fatty acids in ATGL-KO by fatty acid methyl ester (FAME) measurement in a GC-MS experiment. These data suggest that there is a link between changes in lipid hydrolysis and lung cancer progression.

## 1.5. Aim of the research stay

Despite the amount of data that point towards a role of ATGL-KO in the progression of A549 lung carcinoma cells, a more thorough investigation of lipid hydrolysis enzyme manipulation in a panel of lung cancer cell lines is required in order to make a more general statement about the role of intracellular lipid hydrolysis in lung cancer.

To this end, the first aim of the research fellowship in the lab of Matthew Vander Heiden at the Koch Institute of Integrative Cancer research of MIT was to generate a panel of non-small cell lung cancer cell lines with ATGL or MGL deletion to represent lipolysis-deficiency. The use of CRISPR-Cas9 technology to generate additional lipolysis-deficient cell line models would greatly benefit the quality and validity of the research project. Investigation and manipulation of ATGL in additional models would help decipher whether the loss of ATGL and the previously observed subsequent phenotypic and metabolic changes can be reproduced in the already investigated cell line (A549), and whether these are observations specific to A549 lung carcinoma cells or if the observed changes are a more general phenomenon of lipolysis deficiency on (lung) cancer cells.

Another aim of the research stay was to learn and apply metabolic tracing through non-radioactive isotope tracers and measurement of fatty acids and polar metabolites through GC-MS in the generated cell models. Metabolic tracing is a useful tool to study

the fate of nutrients within cells and thereby helps to understand potential changes in metabolic pathways. If the generation of new lipolysis-deficient cell lines is successful, this method will be applied to the newly generated cell lines.

If the newly generated cell lines corroborate our previous findings, i.e., changed phenotype upon deletion of a lipolysis enzyme, another aim is to investigate the growth of these cell lines as tumors in the lungs of mice, which would be enabled through collaboration with colleagues in the Vander Heiden lab that are proficient in intra-tracheal injection of cell lines into lungs of mice.

# 2. Material and Methods

## 2.1. Cell line models and cell culture conditions

ATGL (*PNPLA2*) and MGL (*MGLL*) knockout was achieved in a panel of NSCLC cell lines (A549, H1299, H358, H441) through CRISPR-Cas9 methodology. In brief, short guide RNAs (sgRNAs) were designed using the CRISPick tool by the Broad Institute (https://portals.broadinstitute.org/gppx/crispick/public). The ssgRNAs were chosen based on their location (same exon, approx. 50-150 base pairs apart) and CRISPick rank. sgRNA oligos (Table 3) were cloned into the pSpCas9(BB)-2A-GFP (#48138, Addgene) (Fig. 1A), pU6-(BbsI)_CBh-Cas9-T2A-BFP (#64323, Addgene) (Fig. 1B), or into the lentiGuide-Puro plasmid (#52963, Addgene) (Fig. 1C). The first two express a fluorophore (GFP or BFP) for selection, while the latter expresses puromycin N-acetyl-transferase gene for puromycin selection. All plasmid backbones (Fig. 1A-C) also express a S. pyogenes sgRNA CRISPR customizable RNA element with a 5' and 3' BbsI restriction enzyme cut site for the introduction of the sgRNA.

In CRISPR-Cas9 approach 1, the deletion of ATGL or MGL in parental cell lines was attempted by transiently transfecting the target cell lines with plasmids containing genetic information for Cas9, a fluorophore (GFP (Fig. 1A) or BFP (Fig. 1B)) and sgRNAs targeting the gene of interest in the genome (Table 3). The plasmids were introduce using Lipofectamine™ 3000 Transfection Reagent (#L3000001), Thermo Fisher) according to the manufacturer's protocol. In a previous experiment, the DNA amount for optimal transfection was determined for each target cell line (Table 2). 48 hours days after transfection, the cells were sorted for high BFP and GFP expression and collected as a polyclonal cell population. For CRISPR-Cas9 approach 2, in a first step, target cell lines were infected with virus expressing the lentiCas9 blast plasmid

(#52962, Addgene) (Figure 1D) - which contains genetic information for the *S. pyogenes* Cas9 as well as the Blasticidin S deaminase gene bsd, both under the EFS-NS promoter – for the generation of target cell lines that stably express Cas9. Cells were selected with 10 µg/ml blasticidin (#A1113903, Thermo Fisher) for a week or until all control cells (not infected with lentiCas9 blas) were dead, and subsequently kept at 5 µg/ml blasticidin. The Cas9 expressing parental cells were then subsequently infected with virus expressing the lentiGuide Puro plasmid containing the sgRNAs and selected with 2 µg/ml puromycin and 5 µg/ml blasticidin for 3 days or until all control cells were dead. Plasmid expressing virus was prepared by transfecting Lenti-X™ 293T cells using the *Trans*IT-VirusGEN® Transfection Reagent (Mirus Bio, #) according to the user manual with following plasmids: pMDLg (Addgene, #12251), pMD2.g (Addgene, #12259), pRSV-REV (Addgene, #12259), and the respective target plasmid (e.g., lentiCas9 blast plasmid or lentiGuide Puro plasmid with sgRNA inserted). All newly generated cell lines are summarized in Table 1. All cell lines were cultured at 37 °C and 5% CO2 in Rosswell Park Memorial Institute-1640 (RPMI) medium with phenol-red and 2 g/L of glucose (RPMI-1640, #R0883, Merck) supplemented with 10% Fetal Bovine Serum (FBS) and with 2 mM L-Glutamine (#25030081, Gibco), and 50 Units/ml Penicillin 50µg/ml Streptomycin (1:100 from #15070063, Gibco). For cultivation in lipid-depleted medium, RPMI medium was supplemented with 10% “lipid-stripped” FBS but otherwise prepared as described above. “Lipid-stripped”/lipid-depleted FBS was prepared according to a bio-protocol publication by Hosios *et al.* [25].

## 2.2. Cell proliferation

For determination of cell counts, cells were plated at roughly 15,000 cells per well of a 12-well plate and allowed to attach overnight. Cell counts were determined at timepoint 0 and after 24-96 hours (depending on proliferation rate) using a Multisizer 3 Coulter Counter (Beckman Coulter) with diameter settings between 10µm and 30µm.

## 2.3. 3D cell culture

For the determination of doubling times in 3D cell cultures, cells were plated at 10,000 cells per well in 200 µl of medium into an Ultra-Low Attachment 96-well Plate (#7007, Corning). Spheroid formation was induced by centrifugation at 1,200 rpm for 20 minutes. The cells were kept in culture for 11 days with medium exchange on days 4 and 8 (post plating). Cells were counted on days 0, 8, and 11 post plating. For cell counts, spheroids were washed once in PBS and suspended in 100µl Trypsin. After 5 minutes, cell suspension was pipetted up and down to dissociate the spheroid, and 100µl of medium was added to quench the trypsin reaction. Cell counts were determined as described in the previous section.

## 2.4. Western Blot

For validation of ATGL and MGL KO cell lines, western blotting was performed. Cells were harvested in RIPA buffer (#BP-115, Boston BioProducts) constituted with 1:100 Protease/Phosphatase Inhibitor (#78440, Thermo Fisher). Protein quantification was performed using a Bradford protein assay (#5000006, Biorad) with BSA as standard. The separation of proteins was done on precast Invitrogen™ Bolt™ 4-12% Bis-Tris Plus Gels followed by blotting of the proteins onto a 0.45µm nitrocellulose membrane in a wet

chamber at 30V for 16 hours. Unoccupied sites on the membrane were blocked by 5 % skim milk in Tris-buffered saline containing 0.1 % Tween 20 (TBS-T). Following primary antibodies were used: ATGL (#2138S, Cell Signaling Technologies), MGL (#PA5-27915, Thermo Fisher), Vinculin (#4650, Cell Signaling Technologies). Primary antibodies were diluted 1:1000 in 5 % BSA (ATGL, MGL) or 1:5000 in 5 % BSA (Vinculin). Incubation with primary antibody solutions was performed overnight at 4° C on a shaker. Membranes were washed with TBS-T thrice, followed by incubation for 1 hour at room temperature with diluted (1:5000) secondary antibody in TBS-T: anti-rabbit horseradish peroxidase (HRP)-linked antibody (Cell Signaling Technology). The bands were detected on an ImageQuant™ LAS4000 biomolecular imager (GE Healthcare) after application of Clarity Western ECL Substrate (#1705061, Biorad). Analysis of acquired images was performed by ImageJ (1.54d version, Java 1.8.0_345 version).

## 2.5. Flow cytometry

For functional validation of ATGL-KO, flow cytometry was used to determine the relative lipid droplet content of the generated cell lines according to a 2017 protocol by Qiu and Simon on neutral lipid staining in Bio Protocol Journal [26]. Briefly, cells were plated in a 6-well plate to reach 70-90% confluency the next day. Cells were washed with PBS twice and incubated with 2µM BODIPY™ (#25892, Cayman Chemical Company) in PBS for 15 min at 37°C. Cells were then washed with PBS, trypsinized, quenched with medium and transferred into flow tubes through a 35µm strainer cap to avoid cell clumps. Flow cytometry was performed on a FACS LSR II flow cytometer (BD Biosciences) equipped with a 488 laser and 530/30 filter to assess BODIPY™ intensity. The median of

BODIPY™ positive cells was assessed with the BD FACSDiva software (version 8.0). To test the sensitivity of this method parental cell lines were incubated with 30µM oleic acid-BSA conjugate or 5µM DGAT1 inhibitor (PF-04620110) and 5µM DGAT2 inhibitor (PF-06424439) for 24 hours, as a positive and negative control, respectively.

## 2.6. Metabolic tracing: stable isotope labeling and extractions

For metabolic tracing experiments to trace the fate of glucose into downstream metabolites, RPMI without glucose (#R9011, USBiological Life Sciences) was prepared and reconstituted with [U-$^{13}$C] (=labeled) glucose (#CLM-1396, Cambridge Isotope Laboratories, Inc.) or [U-$^{12}$C] (=unlabeled) glucose, and with regular or delipidated FBS according to Table 4.

Cells were seeded at 50,000 cells per well in a 6-well plate and cultured overnight. Prior to the experiment, the cells were washed three times with PBS and then cultured in 4 ml media containing 11 mM glucose and the indicated treatment condition (i.e., tracing medium or non-tracing medium and lipids or non-lipid medium). At 72h cells in non-tracing medium were counted and cells in tracing medium were harvested. For harvest, cells were washed quickly in cold blood bank saline and lysed in 700µl of lysis buffer. Lysis buffer consisted of Methanol (constituted with 25 mg/l butylated hydroxytoluene) with 0.88% KCl in a ratio of 4:3 (MeOH/KCl). 1.5 µg/ml C17:1 fatty acid was added as internal standard for the extraction of fatty acids. Samples were scraped and transferred into glass vials containing 800µl dichloromethane, followed by 15 min vortex at 4°C. After centrifugation at 3,500 x g for 10 min at room temperature, the lower, lipid-

containing dichloromethane phase was transferred to new glass vials and dried under stream of nitrogen.

## 2.7. FAME derivatization

For fatty acid methyl ester (FAME) derivatizations, the lipid pellets were dissolved in 100 µl toluene. 200 µl of 2% sulfuric acid in MeOH was added and incubated at 50°C overnight. 500 µl of 5% NaCl was added to the samples and extracted twice with 500 µl of hexane. The hexane phases were collected in glass MS vials and dried under nitrogen. The dried samples were dissolved in 50 µl of hexane and measured via GC-MS.

## 2.8. GC-MS metabolite measurement

The GC-MS analysis of polar metabolites was carried out using an Agilent 7890 gas chromatograph (GC) equipped with a 30-meter DB-35MS capillary column (30m x 0.25mm x 0.25µm, Agilent J&W Scientific) coupled to an Agilent 5975C mass spectrometer (MS) operating under electron impact ionization at 70 eV. 1 µl of sample was injected in 1:1 split mode at a temperature of 270°C. Helium was used as the carrier gas at a flow rate of 1 ml/min and the gradient was as follows: 100°C for 5 min and then subsequently heated to 300°C at a rate of 3.5°C/min. For the measurement of fatty acid methyl ester (FAME) samples, a DB-FastFAME GC Column, 30m x 0.25mm x 0.25µm, Agilent J&W Scientific) was used in an Agilent 7890 GC coupled to an Agilent 5975C MS. Separation was carried out using a temperature gradient starting at 100°C for 5 min, increasing to 180°C at 8°C/min, followed by a ramp to 230°C at 1°C/min. For data

analysis, the raw data were converted to .mzML files using MSConvert (ProteoWizard), corrected for naturally occurring isotopes using an in-house R script and subsequently analyzed using El maven.

# 3. Results

## 3.1. Generation of NSCLC cell lines lacking ATGL or MGL

During the research stay in the lab of Matthew Vander Heiden at MIT, new CRISPR-Cas9 methods were acquired. The CRISPR-Cas9 methods, which are more thoroughly explained in the material and methods part 2.1, were used on several non-small cell lung cancer cell lines and were employed for the manipulation of two enzymes involved in intracellular lipid hydrolysis: adipose triglyceride lipase (ATGL) and monoglyceride lipase (MGL). The parental cell lines were selected based on their histological (sub-)subtype and genetic background and include the following: A549, NCI-H1299 (short: H1299), NCI-H358 (short: H358), and NCI-H441 (short: H441). The characteristics of the parental cell lines and the generated KOs are summarized in Table 1. For the generation of CRISPR-mediated knockout of ATGL or MGL, two approaches were used. CRISPR-Cas9 approach 1, in which sgRNA and fluorophore-containing plasmids were introduced into the target cells by lipofectamine, followed by selection of double positive cells (high GFP and BFP signal) through flow cytometry, did not cause reduced expression of the targets (ATGL, MGL) in the polyclonal population of both tested cell lines, A549 (Fig. 1E) and H1299 (Fig. 1F).

In CRISPR-Cas9 approach 2, Cas9 was first stably introduced into the parental cell lines, followed by introduction of sgRNAs targeting ATGL or MGL. The resulting polyclonal populations were subjected to KO validation by western blot. In all four tested cell lines, ATGL expression was abolished upon ATGL-KO and MGL was abolished in MGL-KO polyclonal cell lines (Fig. 1G-J). The cell lines generated with this, second, CRISPR-Cas9 approach (Cas9 cell lines) were used for further experiments.

## 3.2. Deletion of ATGL leads to lipid droplet accumulation

Deletion of ATGL, the main enzyme degrading triglycerides intracellularly, is expected to cause significant accumulation of lipid droplets. Therefore, we next sought to determine whether ATGL deletion indeed renders the cell lines lipolysis deficient and causes accumulation of lipid droplets. To this end, a flow cytometry-based lipid droplet staining and quantification protocol was developed in the Vander Heiden lab. The protocol was based on a bio-protocols publication employing the green fluorescent dye bodipy that stains lipids and lipophilic compounds [26]. As a functional validation of the ATGL-KOs, lipid droplet staining and analysis using flow cytometry was employed. To test the ability of lipid droplet depletion and induction in the parental cell lines, the four different cell lines, A549, H1299, H358, and H441 were first treated with 5μM DGAT1 inhibitor and 5μM DGAT2 inhibitor for 24 hours (DGATi), or with 30μM oleic acid-BSA conjugate (Oleic Acid), to prevent lipid droplet formation or induce accumulation of lipid droplets. As a control, cells were treated with vehicle (DMSO). After 24 hours, the lipid droplets were quantified by flow cytometry and are given as mean bodipy intensity. The different cell lines show different basal lipid droplet levels (Figure 2A). While all of them showed lipid droplet accumulation upon treatment with oleic acid, they did not increase their lipid droplet content to a similar degree. Compared to vehicle control, both H1299 and H358 showed almost 3-fold increase in median bodipy intensity, while A549 cells approximately doubled the median intensity of bodipy signal. The least striking change was observed in H441 cells upon oleic acid treatment. Inhibition of lipid droplet formation by DGAT inhibitors, on the other hand, reduced lipid droplet signal in all the cell lines and the change is more similar in the cell lines for reduction of bodipy signal. Only in A549 cells the DGAT inhibition caused very little reduction in median bodipy intensity. In

Figures 2B-E, the median bodipy intensity and thus lipid droplet content in control (NTC) and ATGL deficient (ATGL) Cas9 expressing polyclonal cell lines is represented. In all four tested cell lines, the deletion of ATGL resulted in increased bodipy signal. These findings further corroborate a successful ATGL deletion and deficiency in breaking down intracellular lipid droplets. The biggest difference in bodipy signal between controls and ATGL-KO cells was observed in H441 cells (64%, Fig. 2E), followed by A549 (40% increase, Fig. 2B) and H1299 (28%, Fig. 2C), while there was only a small increase in H358 cells (8%, Fig. 2D).

It should be noted that representative experiments are shown in Figure 2 for all lipid droplet analyses, and that the basal level of bodipy intensity in parental or control (NTC) cell lines was different across different experiments. While in each experiment the same trends were observed (e.g., oleic acid treatment or ATGL deletion causes increased bodipy intensity, while DGATi causes a decrease), no conclusions can be made about the basal level of lipid droplets in different cell lines until all of them are measured at the same time. Additionally, it would be beneficial to also determine the lipid droplet accumulation and content microscopically.

## 3.3. Deletion of ATGL or MGL causes changes in proliferation

Since we previously observed proliferation increase in A549 cells upon deletion of ATGL, the proliferation of control (NTC) and KO cell lines was assessed. Polyclonal A549 ATGL-KO cells generated in the course of this research stay showed a similar increase in proliferation compared to control (NTC) cells, in both 2D cell culture (Fig. 3A/E) and 3D cell culture (Fig. 3H). Similarly, MGL-KO increased proliferation compared

to controls, and the increase is more striking in 3D cell culture (Fig. 3H) compared to 2D cell culture (Fig. 3A). We observed a similar phenotype in H1299 cells, were ATGL-KO caused increase in proliferation in 2D (Fig. 3B/F) and 3D cell culture (Fig. 3I) and MGL-KO also caused increase in proliferation, although to a smaller extent in 2D (Fig. 3B) as well as 3D (Fig. 3I). H358 cells on the other hand showed no increase in proliferation upon ATGL-KO or MGL-KO, if anything the lipolysis deficiency decreases the proliferation in this cell line (Fig. 3C/G). In the generally more slowly proliferating cells H441, the deletion of ATGL but not MGL increases proliferation slightly (Fig. 3D).

A549 and H1299 show higher proliferation rates compared to the other two tested cell lines, H358 and H441 (Fig. 3J), and thus the generation of ATGL-KO and MGL-KO was attempted and achieved first in A549 and H1299 background. These cells have therefore been more thoroughly tested (e.g., 3D cell culture (A549, H1299) and metabolic tracing (A549)).

## 3.4. ATGL inhibitor increases expression of ATGL

Recently, a small molecule inhibitor against human ATGL – NG-497 – was established [27]. We aimed to test the effect of ATGL inhibition by this inhibitor in the parental cell lines that were also used to generate ATGL-KO cell lines. In contrary to the observations made in the polyclonal ATGL-KO cell lines, where proliferation increased in most cell lines upon ATGL deletion, the inhibition of ATGL caused little change in proliferation or even slightly decreased proliferation (Fig. 4A-D). We further tested lipid droplet content in parental cell lines after treatment with ATGL inhibitor. Lipid droplet content did not increase to a similar extent as when compared to deletion of ATGL through CRISPR-Cas9. In A549 cells, lipid droplet signal increased by 20% (Fig. 4E) and thus to a lesser

extent then with ATGL-KO (Fig. 2B). Treatment with ATGL inhibitor in H1299 and H441 cells only increased bodipy signal marginally, by 1.5% (Fig. 4F), or 4.3% (Fig. 4H) in H1299 or H441 cells, respectively. The only exception is H358, where ATGL inhibitor treatment increased the media bodipy signal and thus lipid droplet content by roughly 20% (Fig. 4G), while it was only 8% upon ATGL-KO.

Given these findings, we sought to understand why ATGL inhibitor treatment mostly could not increase lipid droplet content to the same extent as ATGL deletion, and why the cells did not show similar phenotypic differences (i.e., changes in proliferation). We checked ATGL expression upon ATGL inhibition in the cell lines. Strikingly, we observed that ATGL expression increases in the cells treated with ATGL inhibitor, with exception of H1299, where expression decreases (Fig. 4I/J). We hypothesize that the cells increase ATGL expression as a compensatory mechanism, but exactly how these cells enable this compensatory mechanism and how H1299 cells behave differently has yet to be answered. In order to fully understand this discrepancy between genetic manipulation of ATGL and the inhibitor treatment, additional experiments need to be performed.

In this study, we proceeded with the genetically manipulated cell lines.

## 3.5. ATGL or MGL deletion does not make lung cancer cells dependent on exogenous lipids

With the deletion of ATGL or MGL, the mobilization of fatty acids from triglyceride stores within the cells is disturbed. We hypothesize that cells are more dependent on de-novo fatty acid synthesis or on supply of exogenous fatty acids under these circumstances. We aimed to test the effect of growing cells in medium stripped of lipids, i.e., lipid-depleted medium or “- lipids”. Cells were grown in -lipid or +lipid conditions and

proliferation was assessed. Growing A549 parental (Fig. 5A) as well as H1299 parental (Fig. 5B) in lipid depleted medium did not cause extensive changes in proliferation. H358 parental cells grew slightly slower in lipid depleted medium (Fig. 5C). H441 cells, on the other hand, appear to thrive in lipid stripped medium and increase their proliferation (Fig. 5D). In A549 Cas9 polyclonal cell lines, the control cells as well as the ATGL-KO and MGL-KO cell lines show decreased proliferation in lipid depleted medium (Fig. 5E). The proliferation of H1299 Cas9 polyclonal cell lines appears unchanged upon growth in lipid depleted medium (both ATGL-KO and MGL-KO). However, the H1299 Cas9 polyclonal control cells show decreased proliferation when grown without exogenous lipids (Fig. 5F). Overall, these findings highlight that all the cell lines that were used in this study can grow in lipid depleted conditions without severe proliferation deficiency. Furthermore, we hypothesize that upon ATGL or MGL deletion, the cells grown in lipid depleted medium rely more on de-novo fatty acid synthesis compared to control cells, that also have the chance to mobilize fatty acids from triglyceride stores. To this end, we next performed metabolic tracing of A549 Cas9 polyclonal cell lines with ATGL-KO or MGL-KO or controls to assess the rate of fatty acid synthesis from glucose.

It should be noted that the lipid depleted medium was prepared with delipidated medium, while the control medium contained dialyzed FBS and thus the FBS was from different batches. In a more controlled set of experiments, the +lipid medium should be prepared with the same batch delipidated FBS and lipids should be added back to the medium. This would guarantee similar levels of other FBS contents (e.g., growth factors) that might influence cell proliferation.

## 3.6. Metabolic tracing of uniformly $^{13}$C-glucose into fatty acids

To test our hypothesis, that cells with ATGL deletion or MGL deletion that are grown in lipid depleted medium are more dependent on de-novo fatty acid synthesis, we performed a metabolic tracing experiment. In this experiment, the cells were grown for 72 hours in medium containing lipids (+ lipids) or not (- lipids), and uniformly labelled $^{13}$C-glucose was used as the sole glucose source. After 72 hours, the cells were counted, and fatty acid methyl ester (FAME) extraction was performed. The first fatty acid generated by de-novo fatty acid synthesis is the saturated fatty acid palmitate (C16:0) [28]. We here show palmitate labelling as a representation of de-novo synthesized fatty acids in general. Figure 6 shows unlabelled palmitate levels (Fig. 6A/C) as well as fraction distributions of labelled palmitate (Fig. 6B/D). Fractions of palmitate are denoted as m+n, where n is the number of carbon atoms derived from labelled glucose. Fractions with increasing number of labels thus have been generated through de-novo fatty acid synthesis with glucose as the carbon source. The fraction of unlabelled palmitate was generally higher in cells grown in +lipid medium (Fig. 6A) compared to cells grown in -lipid medium (Fig. 6C). Correspondingly, the overall sum of fractions of palmitate that was derived to some degree from de-novo fatty acid synthesis was higher in all cell lines grown in lipid depleted media, which corroborates our hypothesis that cells grown in lipid depleted media rely on de-novo fatty acid synthesis to a larger degree. More importantly, when looking at the fractional distribution of palmitate it becomes apparent that in both cell lines with lipase deletion (ATGL, MGL) compared to control (NTC) the fraction distribution is shifted to the right, meaning a larger fraction of palmitate that contains a large number of carbons derived from glucose (Fig. 6B/D). This concomitantly

represents that a larger fraction of fatty acids is derived from de-novo fatty acid synthesis. This shift of fractional distribution in lipolysis deficient cells is observed in cells grown in lipid containing (Fig. 6B) as well as in lipid deficient medium (Fig. 6D). However, the overall fraction of palmitate derived from glucose is larger in cells grown in lipid deficient medium. These findings suggest that, irrespective of the presence of exogenous lipids, A549 cells with deletion of an intracellular lipase (ATGL or MGL) generate more of their fatty acids from de-novo synthesis compared to control cells.

# 4. Discussion

The findings from this study provide valuable insights into the role of intracellular lipid catabolism enzymes, specifically ATGL and MGL, in cancer progression and metabolism. The previous observation of increased proliferation and migration in ATGL-knockout A549 lung cancer cells in 2D culture and more strikingly in 3D cell culture[16,24] was reproduced in A549 cells upon ATGL deletion by new CRISPR-Cas9 techniques. A similar phenotype is also observed upon deletion of MGL. These observations highlight the importance of ATGL- and MGL-mediated lipolysis in regulating the behavior of lung cancer cells.

Previously, proteomic analysis of the ATGL-knockout spheroids revealed alterations in glucose and fatty acid metabolism, which were consistent with increased expression of glucose transporters and higher lactate levels. These findings suggest a metabolic rewiring in lipolysis-deficient cells, potentially compensating for the impaired lipid catabolism. The higher levels of monounsaturated fatty acids further support dysregulated lipid metabolism in the absence of ATGL. However, it should be noted that the correlation between lipid droplet accumulation and proliferation requires further investigation through additional experiments.

In this study, we demonstrate that the deletion of ATGL generally leads to increased proliferation in lung cancer cell lines like A549, H1299 and H441, with exception of H358 cells, which interestingly also showed the least lipid droplet accumulation. This discrepancy might indicate a complex relationship between lipid metabolism and cell proliferation that warrants further exploration. Additional experiments focusing on the

metabolic differences between H358 cells and comparing their lipid metabolism and proliferation rates to other cell lines could shed light on this observation.

Metabolic tracing using stable-isotope labeled metabolites provided valuable insights into how lipolysis deficiency (through ATGL- or MGL-KO) influences the metabolism of the generated cell lines. The data revealed an increase in de-novo fatty acid synthesis in cells lacking ATGL or MGL, two enzymes important in intracellular lipolysis. This finding suggests a compensatory mechanism in these cells to maintain fatty acid availability for various cellular processes. Further investigation can be conducted to determine the fatty acid synthesis rate through enzymatic assays or by assessing the expression level of FASN (fatty acid synthase). Additionally, inhibiting FASN in the cell lines could provide insights into the impact of fatty acid synthesis inhibition on their behavior.

Additionally, the NAD(P)+/NAD(P)H ratio of the cell lines in basal state, or upon growth in lipid-containing or lipid-depleted medium could be assessed to explore potential alterations in cellular redox status. Dysregulated lipid metabolism may impact cellular redox homeostasis, and studying the NAD(P)+/NAD(P)H ratio could provide further understanding of this aspect.

In conclusion, the results of this study support the crucial role of intracellular lipid catabolism enzymes, particularly ATGL and MGL, in lung cancer progression and metabolism. Deletion of ATGL or MGL was associated with increased proliferation in most cell lines, while metabolic alterations indicated a compensatory shift in glucose and fatty acid metabolism. Further investigations, including exploring the correlation between lipid droplet accumulation and proliferation in H358 cells, examining fatty acid synthesis rate, inhibiting FASN, and assessing cellular redox status, will deepen our understanding

of the complex interplay between lipid metabolism and cancer. These findings contribute to the growing field of cancer metabolism and provide potential targets for therapeutic interventions.

## 5. Take away from the research stay and future directions

The research stay in the lab of Professor Matthew Vander Heiden at Koch Institute for Integrative Cancer Research of MIT was a great opportunity, not only from a scientific perspective but a personal one as well. At this point, I want to thank Matthew Vander Heiden and everyone in the lab that I have met for their kind support and for welcoming me in the lab in such a nice way. I will never forget this period in my life, which helped me grow in many ways. A special shoutout goes to Keene, a graduate student in the lab, who mentored me during my time there and who helped me with everything in the lab (from generating cell lines, learning more about CRISPR techniques, involving me in his own projects and thus enabling me to learn even more, the tracing experiment, …), but more importantly, who is a great person to work with and spend time with.

My research goals in the beginning of the research stay were vast (generation of new lipolysis-deficient cell lines, metabolic tracing, in-vivo model of lipolysis-deficient lung tumor). While the generation of a whole panel of new lung cancer cell lines with either ATGL or MGL deletion was accomplished despite several approaches and initial troubles, the in-vivo experiment failed. We aimed to investigate the growth of tumors derived from cells expressing both ATGL and MGL (e.g., control cells) or lacking either ATGL or MGL and hypothesized, based on 2D and 3D cell culture data, that both tumors lacking a lipolysis enzyme would grow at a higher rate in mouse lungs. Unfortunately,

the injected cell lines did not develop into tumors even after 14 weeks. Since this was the first attempt of an experiment like this with these cell lines, further testing and optimization is required.

For one of the main goals of this research stay – to learn more about metabolic tracing and finally employ this technique – there could not have been a better lab to join than then Vander Heiden lab. The members of the lab do not only perform a lot of tracing experiments, but they critically think and discuss about data analysis and interpretation as well as other related caveats in metabolic tracing experiments. This definitely helped broaden my understanding of this technique and I am grateful to all the lab members who helped me with my experiments and were there to discuss the data.
The acquired knowledge and skills will now be put to use in the home institution and a similar metabolic tracing pipeline will be set up. This will allow metabolic tracing experiments similar to the one reported here for all the other generated cell lines (e.g., H1299, H358, H441 polyclonal control, ATGL-KO or MGL-KO cell lines).

To further characterize the generated cell lines, the glucose and lactate content in the media of the cells grown in 2D as well as in 3D will be measured to determine the glucose consumption and lactate production. Furthermore, LC-MS/MS based proteomics, lipidomics and metabolomics analyses will be employed in the home institute to complement the tracing and phenotype data that was obtained during the research stay.

# 6. Tables

**Table 1: list of generated cell lines**

| parental cell line | Lineage | Lineage Subtype | Lineage Sub-subtype | Mutations | code | Cas9 expression | comments |
|---|---|---|---|---|---|---|---|
| A549 | Lung, primary | NSCLC | Lung Adenocarcinoma | KRAS (p.G12S), STK11 (p.Q37*), TP53 (WT), KEAP1 (p.G333C) | A549 Cas9 NTC | ✓ | ATGL, MGL expression confirmed |
| | | | | | A549 Cas9 ATGL-KO | ✓ | No ATGL expression: **KO confirmed** |
| | | | | | A549 Cas9 MGL-KO | ✓ | No MGL expression: **KO confirmed** |
| | | | | | A549 GFP/BFP NTC | x | ATGL, MGL expression confirmed |
| | | | | | A549 GFP/BFP ATGL-KO | x | ATGL expression: **no KO** |
| | | | | | A549 GFP/BFP MGL-KO | x | MGL expression: **no KO** |
| H1299 | Lung, metastatic | NSCLC | Large Cell Lung Carcinoma | NRAS (Q61K), STK11 (WT), TP53 (WT), KEAP1 (WT) | H1299 Cas9 NTC | ✓ | ATGL, MGL expression confirmed |
| | | | | | H1299 Cas9 ATGL-KO | ✓ | No ATGL expression: **KO confirmed** |
| | | | | | H1299 Cas9 MGL-KO | ✓ | No MGL expression: **KO confirmed** |
| | | | | | H1299 GFP/BFP NTC | x | ATGL, MGL expression confirmed |
| | | | | | H1299 GFP/BFP ATGL-KO | x | ATGL expression: **no KO** |
| | | | | | H1299 GFP/BFP MGL-KO | x | MGL expression: **no KO** |
| H358 | Lung, primary | NSCLC | Lung Adenocarcinoma | KRAS (p.G12C), STK11 (WT), TP53 (WT), KEAP1 (WT) | H358 Cas9 NTC | ✓ | ATGL, MGL expression confirmed |
| | | | | | H358 Cas9 ATGL-KO | ✓ | No ATGL expression: **KO confirmed** |
| | | | | | H358 Cas9 MGL-KO | ✓ | No MGL expression: **KO confirmed** |
| H441 | Lung, metastatic | NSCLC | Lung Adenocarcinoma | KRAS (p.G12V), STK11 (WT), TP53 (p.R158L), KEAP1 (WT) | H441 Cas9 NTC | ✓ | ATGL, MGL expression confirmed |
| | | | | | H441 Cas9 ATGL-KO | ✓ | No ATGL expression: **KO confirmed** |
| | | | | | H441 Cas9 MGL-KO | ✓ | No MGL expression: **KO confirmed** |

**Table 2: DNA amount for optimal lipofectamine transfection (per well of a 12-well plate)**

| target cell line | A549 | NCI-H1299 | NCI-H358 | NCI-H441 |
|---|---|---|---|---|
| DNA amount (ng) | 250 | 1000 | 750 | 1000 |

**Table 3: sequences of sgRNAs for cloning into plasmid backbones**

| Species | Gene | Use | Primer Name | Sequence (5'-3') | Backbone: | Enzyme | Plasmid |
|---|---|---|---|---|---|---|---|
| Hs | PNPLA2 | sgRNA | KA672_HsPNPLA2_1_F | caccgCATTCTCGCCGTCTGACACG | pSpCas9(BB)-2A-GFP (PX458) | BbsI | pSH1: Cas9-GFP-KA672-3 |
| Hs | PNPLA2 | sgRNA | KA673_HsPNPLA2_1_R | aaacCGTGTCAGACGGCGAGAATGc | | BbsI | |
| Hs | PNPLA2 | sgRNA | KA674_HsPNPLA2_2_F | caccgGGCTGGTGCCAAGTTCATTG | pU6-(BbsI)_CBh-Cas9-T2A-BFP | BbsI | pSH2: Cas9-BFP-KA674-5 |
| Hs | PNPLA2 | sgRNA | KA675_HsPNPLA2_2_R | aaacCAATGAACTTGGCACCAGCCc | | BbsI | |
| Hs | MGLL | sgRNA | KA676_HsMGLL_1_F | caccgCTGGTGTTCGCCCACGACCA | pSpCas9(BB)-2A-GFP (PX458) | BbsI | pSH3: Cas9-GFP-KA676-7 |
| Hs | MGLL | sgRNA | KA677_HsMGLL_1_R | aaacTGGTCGTGGGCGAACACCAGc | | BbsI | |
| Hs | MGLL | sgRNA | KA678_HsMGLL_2_F | caccgTCCGAGCCAGCTCTTCATAG | pU6-(BbsI)_CBh-Cas9-T2A-BFP | BbsI | pSH4: Cas9-GFP-KA678-9 |
| Hs | MGLL | sgRNA | KA679_HsMGLL_2_R | aaacCTATGAAGAGCTGGCTCGGAc | | BbsI | |
| Hs | PNPLA2 | sgRNA | KA672_HsPNPLA2_1_F | caccgCATTCTCGCCGTCTGACACG | Lentiguide/puro | BbsI | pSH5: LGP-PNPLA2-1 |
| Hs | PNPLA2 | sgRNA | KA673_HsPNPLA2_1_R | aaacCGTGTCAGACGGCGAGAATGc | | BbsI | |
| Hs | PNPLA2 | sgRNA | KA674_HsPNPLA2_2_F | caccgGGCTGGTGCCAAGTTCATTG | Lentiguide/puro | BbsI | pSH6: LGP-PNPLA2-2 |
| Hs | PNPLA2 | sgRNA | KA675_HsPNPLA2_2_R | aaacCAATGAACTTGGCACCAGCCc | | BbsI | |
| Hs | MGLL | sgRNA | KA676_HsMGLL_1_F | caccgCTGGTGTTCGCCCACGACCA | Lentiguide/puro | BbsI | pSH7: LGP-MGLL-1 |
| Hs | MGLL | sgRNA | KA677_HsMGLL_1_R | aaacTGGTCGTGGGCGAACACCAGc | | BbsI | |
| Hs | MGLL | sgRNA | KA678_HsMGLL_2_F | caccgTCCGAGCCAGCTCTTCATAG | Lentiguide/puro | BbsI | pSH8: LGP-MGLL-2 |
| Hs | MGLL | sgRNA | KA679_HsMGLL_2_R | aaacCTATGAAGAGCTGGCTCGGAc | | BbsI | |

**Table 4: Preparation of tracing and non-tracing media**

| **Media to Prepare** | **volume (ml)** | | | | | | |
|---|---|---|---|---|---|---|---|
| | **total** | **RPMI (#R9011)** | **dialyzed FBS** | **delipidated FBS** | **P/S (100x)** | **Gln (200mM)** | **Glucose (mg)** |
| U-13C Glucose + lip | 150 | 132 | 15 | - | 1.5 | 1.5 | **309.9** |
| U-13C Glucose - lip | 150 | 132 | - | 15 | 1.5 | 1.5 | **309.9** |
| U-12C Glucose + lip | 150 | 132 | 15 | - | 1.5 | 1.5 | **300.0** |
| U-12C Glucose - lip | 150 | 132 | - | 15 | 1.5 | 1.5 | **300.0** |

**Table 5: Primer Sequences for qPCR**

| gene | direction | sequence 5' - 3' |
|---|---|---|
| PNPLA2 | forward | GAGATGTGCAAGCAGGGATAC |
| | reverse | CTGCGAGTAATCCTCCGCT |
| LIPE | forward | TCAGTGTCTAGGTCAGACTGG |
| | reverse | AGGCTTCTGTTGGGTATTGGA |
| MGLL | forward | TCGTCAGGGATGTGTTGCAG |
| | reverse | AGGCGAAATGAGTACCATGCC |
| HIG2 | forward | AAGCATGTGTTGAACCTCTACC |
| | reverse | TGTGTTGGCTAGTTGGCTTCT |
| ABHD5 | forward | CACATGGTGCCCTACGTCTAT |
| | reverse | ACAGGTCTGTTGGTGCAAAGA |
| ACTB | forward | CATGTACGTTGCTATCCAGGC |
| | reverse | CTCCTTAATGTCACGCACGAT |
| EEF1A1 | forward | TGTCGTCATTGGACACGTAGA |
| | reverse | ACGCTCAGCTTTCAGTTTATCC |

# 7. Figures

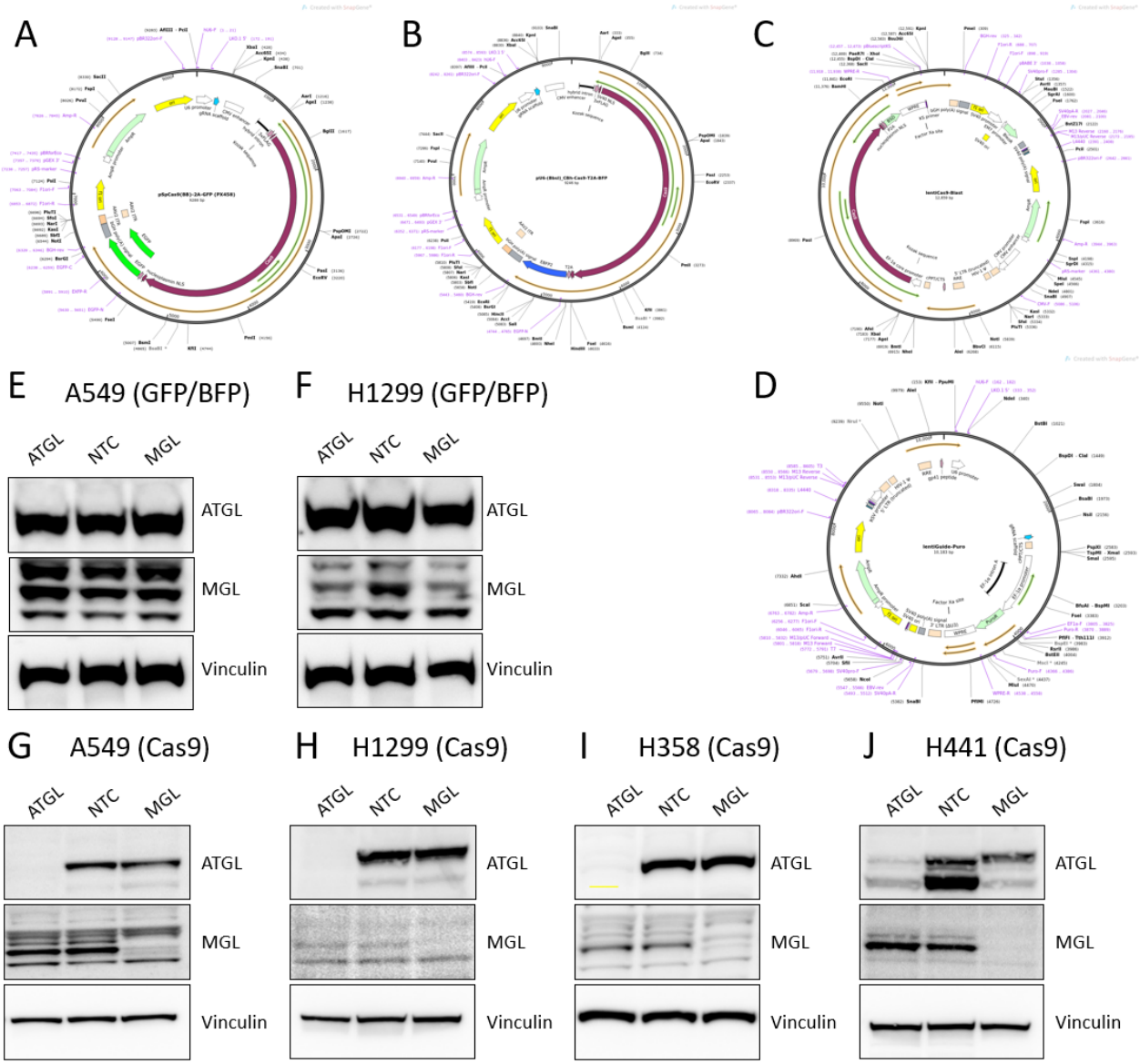


Figure 1: generation of ATGL and MGL KO cell lines. A: plasmid pSpCas9(BB)-2A-GFP, containing Cas9 and GFP; B: plasmid pU6-(BbsI)_CBh-Cas9-T2A-BFP, containing Cas9 and BFP; C: plasmid lentiGuide-Puro, containing puromycin N-acetyl-transferase; D: plasmid lentiCas9 blast, containing Cas9; E (A549 GFP/BFP) and F (H1299 GFP/BFP): western blots showing expression of loading control Vinculin or ATGL or MGL in polyclonal cell lines generated by transfection with plasmids pSpCas9(BB)-2A-GFP and pU6-(BbsI)_CBh-Cas9-T2A-BFP; G (A549 Cas9) H (H1299 Cas9) I (H358 Cas9) and J (H441 Cas9): western blots showing expression of loading control Vinculin or ATGL or MGL in polyclonal cell lines generated in cell lines stably expressing Cas9 by transfection with plasmid lentiGuide-Puro; NTC: non-targeting control, ATGL: ATGL-KO, MGL: MGL-KO.

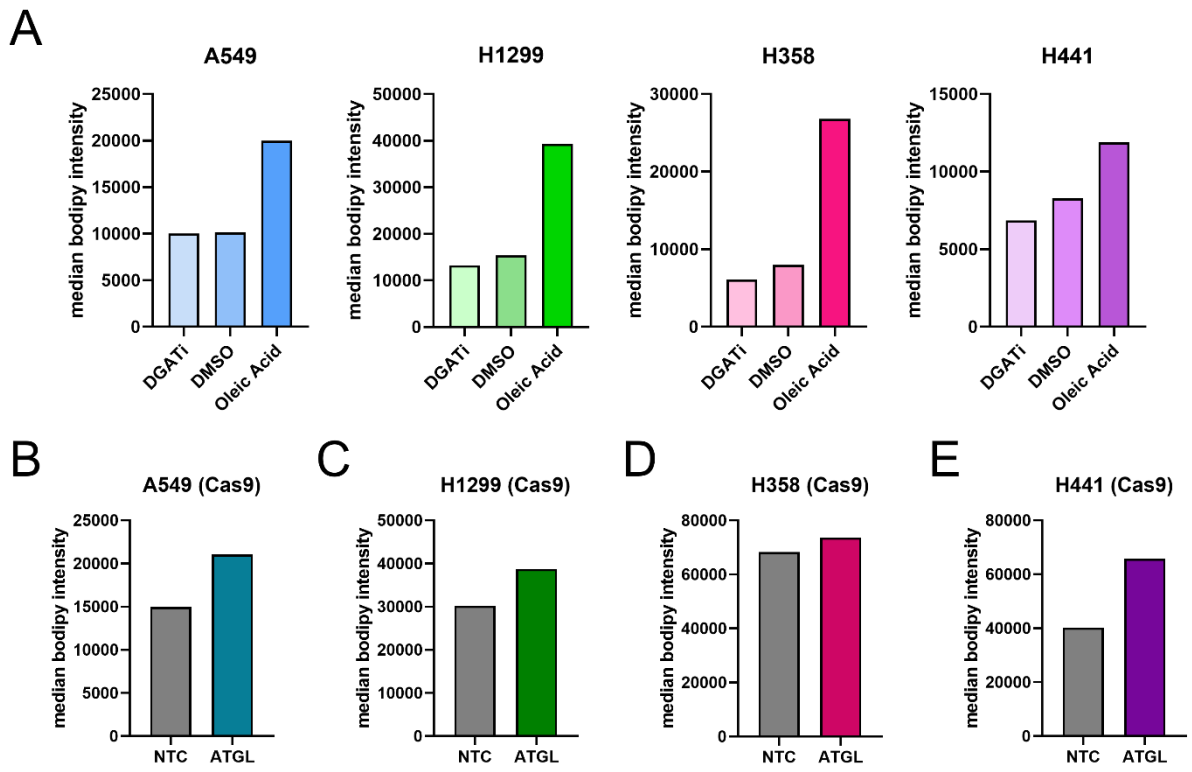


Figure 2: lipid droplet analysis of parental cell lines (A) and Cas9 expressing control and ATGL-KO cell lines (B-E). A: parental cell lines treated with 5µM DGAT1 inhibitor (PF-04620110) and 5µM DGAT2 inhibitor (PF-06424439) to reduce lipid droplets or with 30µM oleic acid-BSA conjugate to induce lipid droplets or DMSO as control; B-E: Cas9 expressing controls (NTC) and ATGL-KO (ATGL) polyclonal cell lines. lipid droplets quantity assessed through staining with bodipy and measurement of the mean fluorescent intensity of cells by flow cytometry

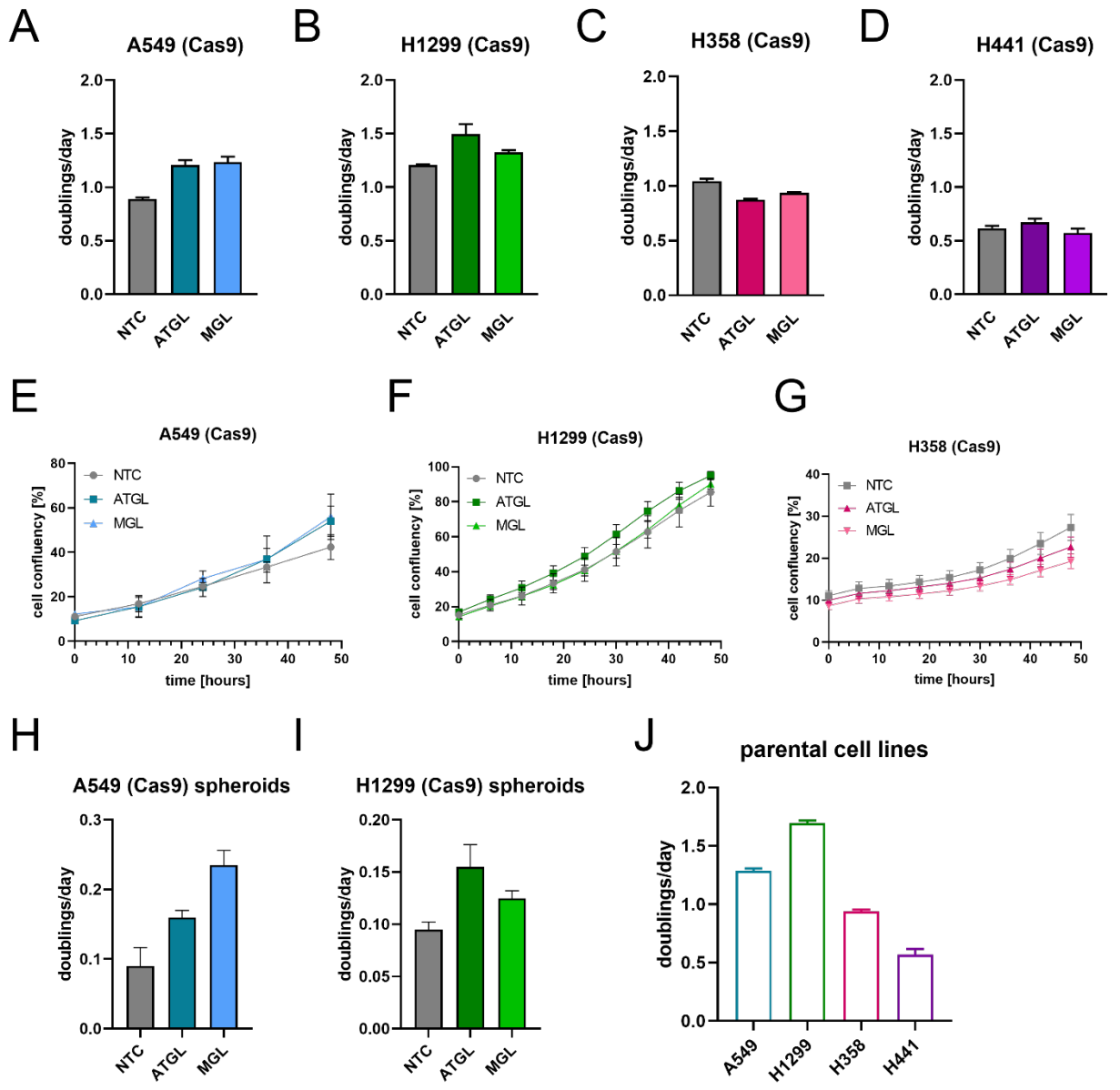


Figure 3: proliferation phenotype of Cas9 expressing polyclonal cell lines in 2D (A-G) and 3D (H-I) and proliferation rate of parental cell lines (J); A (A549) B (H1299) C (H358) and D (H441): cell doublings/day of control (NTC), ATGL-KO (ATGL) and MGL-KO (MGL) Cas9 expressing polyclonal cell lines grown in 2D; E (A549) F (H1299) and G (H358): cell growth rates visualized as cell confluency (%) over time; H (A549) and I (H1299): control (NTC), ATGL-KO (ATGL) and MGL-KO (MGL) Cas9 expressing polyclonal cell lines doublings/day calculated from cell counts over a period of 10 days of cells grown as spheroids in 3D without addition of a supporting matrix; J: cell doublings of parental cell lines grown in 2D. proliferation rate is given as doublings/day and calculated from cell counts at t = 0 hours and t = 48 hours; cell confluency determined by Incucyte® Live-Cell Analysis instrument

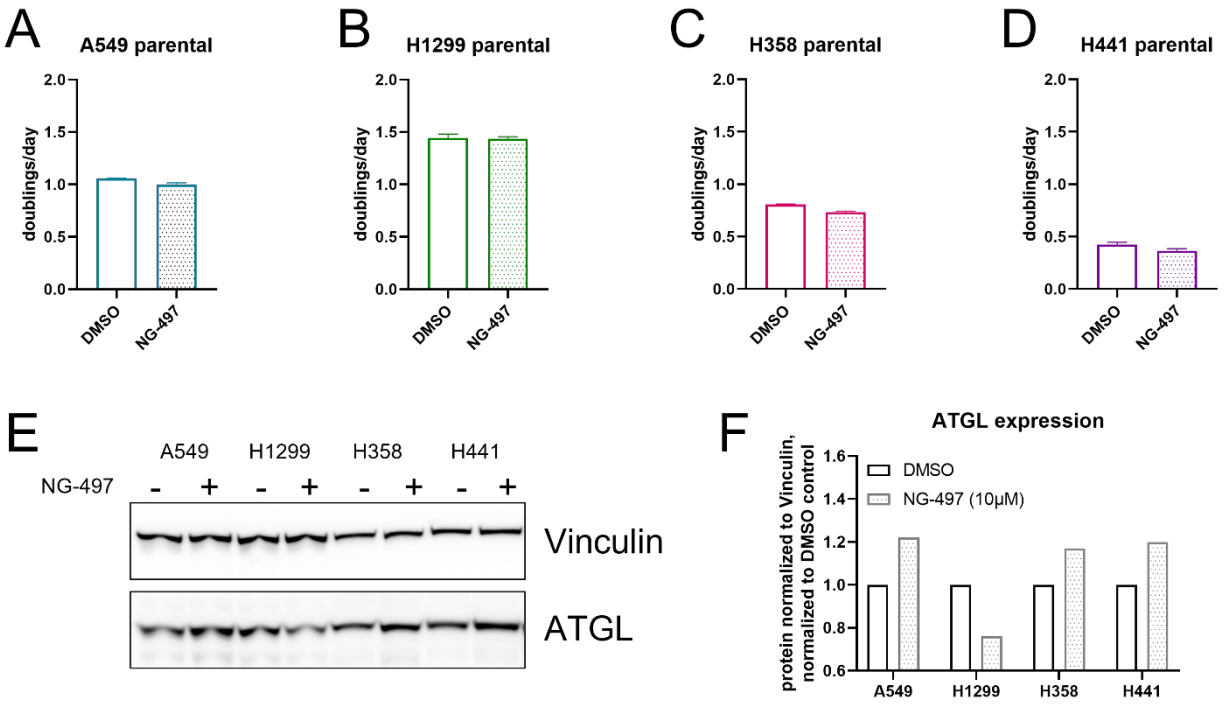


Figure 4: proliferation phenotype of parental cell lines treated with ATGL inhibitor (NG-497). A (A549) B (H1299) C (H358) and D (H441): parental cell lines treated with 10μM NG-497 (human ATGL inhibitor); E: western blots showing expression of loading control Vinculin or ATGL in parental cell lines treated with ATGL inhibitor (+) or vehicle (-); F: quantification of western blot shown in Figure E, ATGL expression normalized to vinculin expression, ATGL inhibitor-treated samples normalized to vehicle treated samples. proliferation rate is given as doublings/day and calculated from cell counts at t = 0 hours and t = 48 hours.

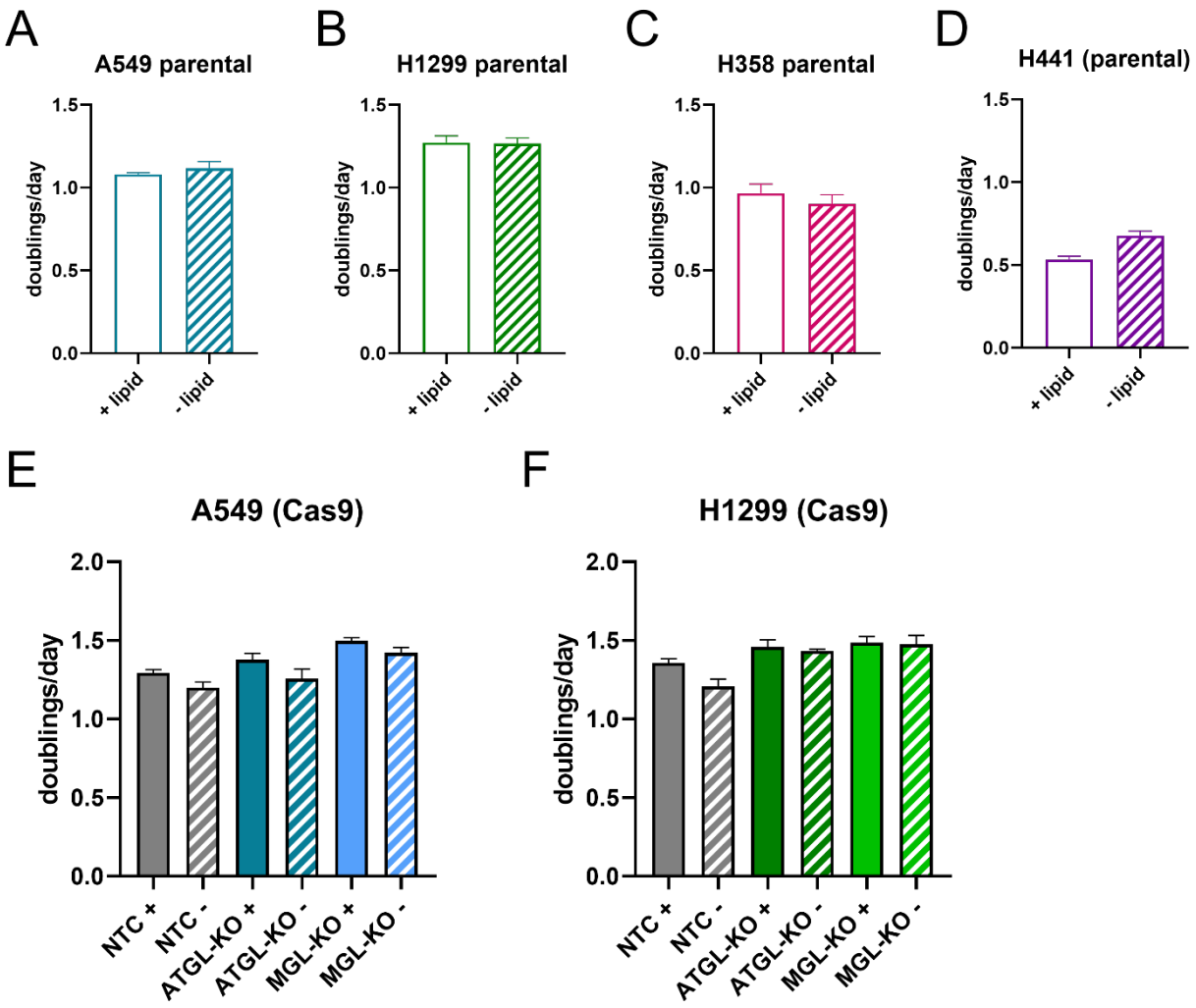


Figure 5: proliferation phenotype of parental cell lines and Cas9 expressing lipolysis-deficient cell lines cultured in normal (+ lipid) or lipid-depleted (-lipid) medium. A (A549) B (H1299) C (H358) and D (H441): parental cell lines cultured in medium containing lyophilized FBS (+lipids) or delipidated FBS (-lipids); E (A549) and F (H1299): A549 Cas9 expressing control (NTC), ATGL-KO (ATGL) and MGL-KO (MGL) polyclonal cell lines cultured in lipid containing or lipid-depleted medium. proliferation rate is given as doublings/day and calculated from cell counts at t = 0 hours and t = 48 hours.

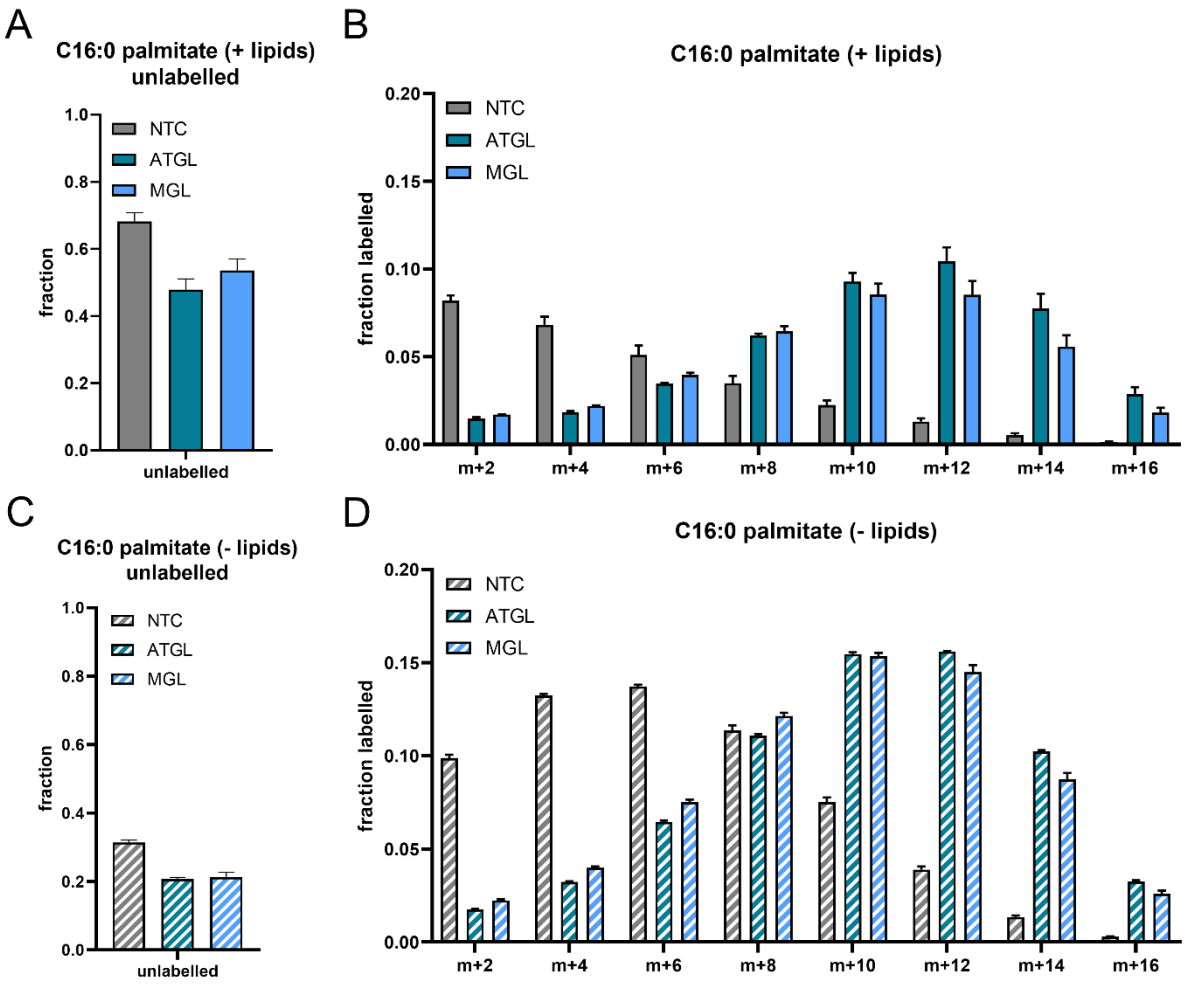


Figure 6: metabolic tracing data of uniformly $^{13}$C-labelled glucose into palmitate. A: the fraction of measured palmitate containing no $^{13}$C-label and thus is not derived from glucose, cells grown in regular (lipid containing) medium; B: distribution of fractions of palmitate with increasing amount of $^{13}$C-label, cells grown in regular (lipid containing) medium; C: the fraction of measured palmitate containing no $^{13}$C-label and thus is not derived from glucose, cells grown in lipid depleted medium; D: distribution of fractions of palmitate with increasing amount of $^{13}$C-label. Fractions are shown as m+n, where n corresponds to the number of $^{13}$C labels derived from glucose that were incorporated. Cells were cultured in respective media for 72 hours, and metabolite levels were normalized to cell counts as well as an internal standard.

# 8. References


1. Bray, F., Ferlay, J., Soerjomataram, I., Siegel, R.L., Torre, L.A., and Jemal, A. (2018). Global cancer statistics 2018: GLOBOCAN estimates of incidence and mortality worldwide for 36 cancers in 185 countries. CA Cancer J Clin *68*, 394-424. 10.3322/caac.21492.
2. de Sousa, V.M.L., and Carvalho, L. (2018). Heterogeneity in Lung Cancer. Pathobiology *85*, 96-107. 10.1159/000487440.
3. Henry, N.L., and Hayes, D.F. (2012). Cancer biomarkers. Mol Oncol *6*, 140-146. 10.1016/j.molonc.2012.01.010.
4. Inamura, K. (2017). Lung Cancer: Understanding Its Molecular Pathology and the 2015 WHO Classification. Front Oncol *7*, 193. 10.3389/fonc.2017.00193.
5. Hanahan, D., and Weinberg, R.A. (2000). The hallmarks of cancer. Cell *100*, 57-70. 10.1016/s0092-8674(00)81683-9.
6. Encyclopedia of Genetics. (2001). (Academic Press).
7. Shortt, J., and Johnstone, R.W. (2012). Oncogenes in cell survival and cell death. Cold Spring Harb Perspect Biol *4*. 10.1101/cshperspect.a009829.
8. Hanahan, D., and Weinberg, R.A. (2011). Hallmarks of cancer: the next generation. Cell *144*, 646-674. 10.1016/j.cell.2011.02.013.
9. Ward, P.S., and Thompson, C.B. (2012). Metabolic reprogramming: a cancer hallmark even warburg did not anticipate. Cancer Cell *21*, 297-308. 10.1016/j.ccr.2012.02.014.
10. Warburg, O., Wind, F., and Negelein, E. (1927). The Metabolism of Tumors in the Body. J Gen Physiol *8*, 519-530. 10.1085/jgp.8.6.519.

11. Currie, E., Schulze, A., Zechner, R., Walther, T.C., and Farese, R.V., Jr. (2013). Cellular fatty acid metabolism and cancer. Cell Metab *18*, 153-161. 10.1016/j.cmet.2013.05.017.

12. Long, J., Zhang, C.J., Zhu, N., Du, K., Yin, Y.F., Tan, X., Liao, D.F., and Qin, L. (2018). Lipid metabolism and carcinogenesis, cancer development. Am J Cancer Res *8*, 778-791. Am J Cancer Res 2018;8(5):778-791.

13. Cruz, A.L.S., Barreto, E.A., Fazolini, N.P.B., Viola, J.P.B., and Bozza, P.T. (2020). Lipid droplets: platforms with multiple functions in cancer hallmarks. Cell Death Dis *11*, 105. 10.1038/s41419-020-2297-3.

14. Itabe, H., Yamaguchi, T., Nimura, S., and Sasabe, N. (2017). Perilipins: a diversity of intracellular lipid droplet proteins. Lipids Health Dis *16*, 83. 10.1186/s12944-017-0473-y.

15. Lass, A., Zimmermann, R., Oberer, M., and Zechner, R. (2011). Lipolysis - a highly regulated multi-enzyme complex mediates the catabolism of cellular fat stores. Prog Lipid Res *50*, 14-27. 10.1016/j.plipres.2010.10.004.

16. Tomin, T., Fritz, K., Gindlhuber, J., Waldherr, L., Pucher, B., Thallinger, G.G., Nomura, D.K., Schittmayer, M., and Birner-Gruenberger, R. (2018). Deletion of Adipose Triglyceride Lipase Links Triacylglycerol Accumulation to a More-Aggressive Phenotype in A549 Lung Carcinoma Cells. J Proteome Res *17*, 1415-1425. 10.1021/acs.jproteome.7b00782.

17. Padmanabha Das, K.M., Wechselberger, L., Liziczai, M., De la Rosa Rodriguez, M., Grabner, G.F., Heier, C., Viertlmayr, R., Radler, C., Lichtenegger, J., Zimmermann, R., et al. (2018). Hypoxia-inducible lipid droplet-associated protein inhibits adipose triglyceride lipase. J Lipid Res *59*, 531-541. 10.1194/jlr.M082388.

18. VandeKopple, M.J., Wu, J., Auer, E.N., Giaccia, A.J., Denko, N.C., and Papandreou, I. (2019). HILPDA Regulates Lipid Metabolism, Lipid Droplet Abundance, and Response to Microenvironmental Stress in Solid Tumors. Mol Cancer Res *17*, 2089-2101. 10.1158/1541-7786.MCR-18-1343.

19. Al-Zoughbi, W., Pichler, M., Gorkiewicz, G., Guertl-Lackner, B., Haybaeck, J., Jahn, S.W., Lackner, C., Liegl-Atzwanger, B., Popper, H., Schauer, S., et al. (2016). Loss of adipose triglyceride lipase is associated with human cancer and induces mouse pulmonary neoplasia. Oncotarget *7*, 33832-33840. 10.18632/oncotarget.9418.

20. Grabner, G.F., Zimmermann, R., Schicho, R., and Taschler, U. (2017). Monoglyceride lipase as a drug target: At the crossroads of arachidonic acid metabolism and endocannabinoid signaling. Pharmacol Ther *175*, 35-46. 10.1016/j.pharmthera.2017.02.033.

21. Nomura, D.K., Long, J.Z., Niessen, S., Hoover, H.S., Ng, S.W., and Cravatt, B.F. (2010). Monoacylglycerol lipase regulates a fatty acid network that promotes cancer pathogenesis. Cell *140*, 49-61. 10.1016/j.cell.2009.11.027.

22. Kienzl, M., Hasenoehrl, C., Maitz, K., Sarsembayeva, A., Taschler, U., Valadez-Cosmes, P., Kindler, O., Ristic, D., Raftopoulou, S., Santiso, A., et al. (2021). Monoacylglycerol lipase deficiency in the tumor microenvironment slows tumor growth in non-small cell lung cancer. Oncoimmunology *10*, 1965319. 10.1080/2162402X.2021.1965319.

23. Liu, R., Wang, X., Curtiss, C., Landas, S., Rong, R., Sheikh, M.S., and Huang, Y. (2018). Monoglyceride lipase gene knockout in mice leads to increased incidence of lung adenocarcinoma. Cell Death Dis *9*, 36. 10.1038/s41419-017-0188-z.

24. Honeder, S., Tomin, T., Nebel, L., Gindlhuber, J., Fritz-Wallace, K., Schinagl, M., Heininger, C., Schittmayer, M., Ghaffari-Tabrizi-Wizsy, N., and Birner-Gruenberger, R. (2021). Adipose Triglyceride Lipase Loss Promotes a Metabolic Switch in A549 Non-Small Cell Lung Cancer Cell Spheroids. Mol Cell Proteomics *20*, 100095. 10.1016/j.mcpro.2021.100095.

25. Hosios, A.M., Li, Z., Lien, E.C., and Heiden, M.V.G. (2018). Preparation of Lipid-Stripped Serum for the Study of Lipid Metabolism in Cell Culture. Bio Protoc *8*, e2876. 10.21769/BioProtoc.2876.

26. Qiu, B., and Simon, M.C. (2016). BODIPY 493/503 Staining of Neutral Lipid Droplets for Microscopy and Quantification by Flow Cytometry. Bio Protoc *6*. 10.21769/BioProtoc.1912.

27. Grabner, G.F., Guttenberger, N., Mayer, N., Migglautsch-Sulzer, A.K., Lembacher-Fadum, C., Fawzy, N., Bulfon, D., Hofer, P., Zullig, T., Hartig, L., et al. (2022). Small-Molecule Inhibitors Targeting Lipolysis in Human Adipocytes. J Am Chem Soc *144*, 6237-6250. 10.1021/jacs.1c10836.

28. Mashima, T., Seimiya, H., and Tsuruo, T. (2009). De novo fatty-acid synthesis and related pathways as molecular targets for cancer therapy. Br J Cancer *100*, 1369-1372. 10.1038/sj.bjc.6605007.